

## ESSD-2021-388 – RC1 comment by Floris Calcoen

We would like to thank the referee for his excellent review, very concise summary and insightful comments on the methodology, limitations, and dataset structure. We appreciate the fact that the referee took the time to download the Github repository and directly test the methodology.

### 1. General comments

#### 1.1. Revisit period and peak tidal frequency

The irregular sampling interval is a very important point, which needs clarification in the manuscript for the benefit of the readers. Three satellites from the Landsat constellation are used in CoastSat to map shorelines: Landsat 5 (1984-2013), Landsat 7 (1999-current), Landsat 8 (2013-current). Theoretically, each satellite has a revisit period of 16 days for every point on Earth (below 80 degrees latitude), so when two satellites are in orbit simultaneously (1999-2019), we should have an 8-day revisit period. As the referee stated, this 8-day sampling interval is the key to this algorithm, as it allows to capture, with a certain degree of aliasing, the fortnightly tidal cycles. Now in practice, there are several factors that, to our knowledge, alter the revisit period of Landsat images (only talking about the images here, not the shorelines):

- i) *Swath overlap*: the Landsat satellites are in a near-polar orbit, where the orbit paths come closer together near the poles. This means that the overlap between images from adjacent swaths increases with latitude, from 7% at the Equator to a maximum of 85% at high latitudes (Department of the Interior U.S. Geological Survey, 2016). Thus, regions located at the edge of the swath will be imaged more frequently. The Landsat scene boundaries (available at <https://www.usgs.gov/media/files/landsat-wrs-2-scene-boundaries-kml-file>), displayed in Figure 1, show that Cable Beach is located in a region of high overlap (both row and path) hence the 0-days and 7-days revisits in addition to the default 8-days revisit period (as shown by the referee's figure) .
- ii) *Availability in Tier 1*: the Landsat images are sorted into Tier 1 and Tier 2 based on whether they meet or not formal geometric and radiometric quality criteria (USGS, 2017). The data provider specifies that only Tier 1 images, which pass the geometric and radiometric quality control, are suitable for time-series analysis.
- iii) *Acquisition strategy*: as the referee rightly pointed out, beyond the Australian scale, the acquisition strategy of the Landsat program was not even across the globe (Wulder et al., 2016), especially for the earlier missions (Landsat 5 and Landsat 7) which required ground receiving stations in line of sight. This results in substantial data gaps in certain regions.

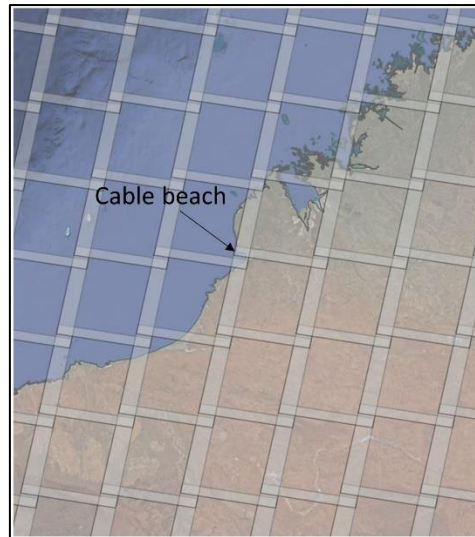


Figure 1. Landsat Scene Boundaries showing the regions of overlap, and the location of Cable Beach in Western Australia.

**Response to a):** The factors mentioned above are the ones that to our knowledge affect the image availability. In addition, there are the issues with the shoreline detection, like clouds, misclassifications, outliers, which also contribute to the unequal temporal distribution of the shoreline time-series.

We have added a sentence briefly describing the reasons for the irregular sampling of the shoreline time-series at **Lines 91-95**. The acquisition strategy and applicability of this method to other geographical areas is addressed in the Discussion.

The 20-year time period (1999-2020) is selected to ensure that two Landsat satellites are in orbit simultaneously, which theoretically results in a combined revisit period of 8 days (16 days for each satellite). However, in practice, time-series of shoreline change are irregularly sampled due to factors such as cloud cover, gaps in Landsat 7 data (scan line corrector error) and discarded images due to poor geometric or radiometric quality. Any outliers in the shoreline time-series (e.g., due to false detections) are also removed using a despiking algorithm.

**Response to b):** The Jupyter Notebook shows an example of how to estimate the beach slope at an individual site. The user can manually select the main sampling period based on the timestep distribution (Figure 2a). If we choose 7 days (Nyquist limit is 14 days), the power spectrum of the tide levels shows a peak at 14.8 days but also a smaller peak at 17.5 days, which results from the aliasing of the 14.8 days cycle with an 8-day sampling period (Figure 2b, also see demonstration of this aliasing in Vos et al. (2020) Supporting Information S3). The algorithm always chooses the frequency with the highest peak on the tidal spectrum to estimate the slopes (with a hard-coded limit at 1 month to only consider high frequencies). If we choose 8 days, the Nyquist limit is 16 days and only the aliased 17.5 days peak is present on the power spectrum (Figure 2c). Note that as we are using a least-squares spectral method (Lomb-Scargle transform), we can design the frequency grid and set its limits and spacing (see discussion in Specific Comments 2).

Now in this example, we get the same slope estimates, whether we use a 7- or 8-days image acquisition interval, we invite the referee to try this on the notebook by changing `settings_slope[`n_days`]=8`. As we didn't observe any differences in this case (only site amongst our validation sites to be in an area of overlap), we have processed the entire dataset with an image acquisition interval of 8 days, which is the theoretical sampling period for two Landsat satellites in orbit simultaneously and should be the most common interval between images.

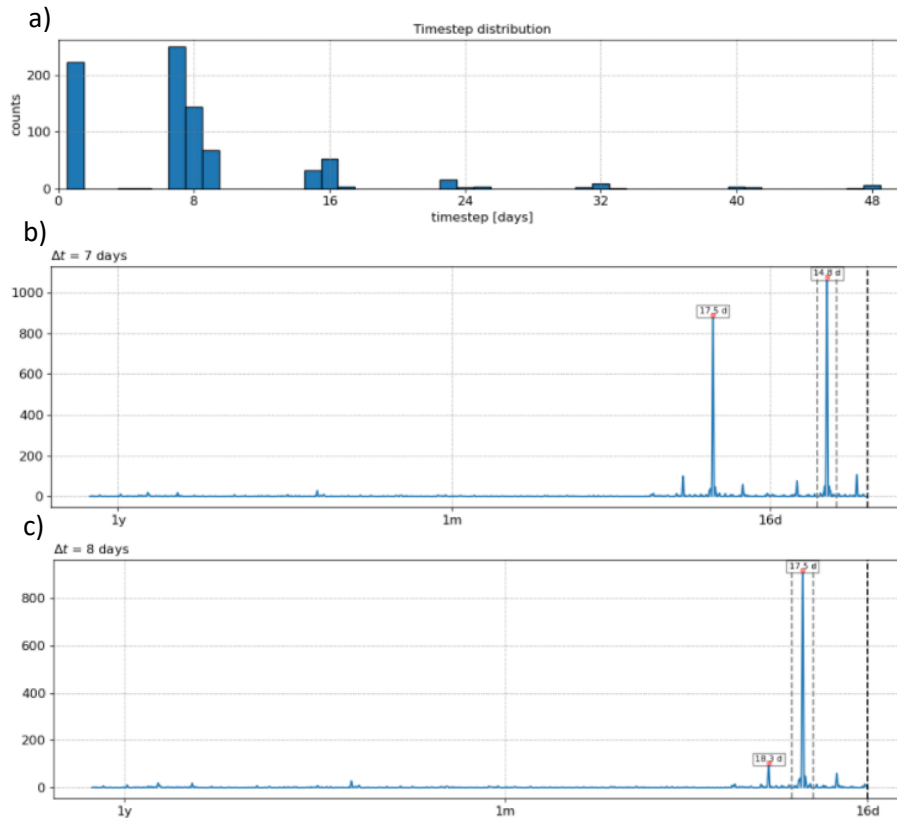


Figure 2. **a)** Distribution of the interval between consecutive images. **b)** Power spectrum density of the tide levels associated with the images using a main sampling period of 7 days (Nyquist limit of 14 days). **c)** same with a main sampling period of 8 days (Nyquist limit of 16 days).

We have addressed this procedure in more detail in the manuscript and have expanded at **lines 98-105**:

Since the Lomb-Scargle is a least-squares spectral method, the limits and spacing of the frequency grid need to be first defined. Here, a main sampling period of 8 days (i.e., the theoretical Landsat revisit period) is used, resulting in a maximum frequency (Nyquist limit) of 16 days, and the spacing  $n_0$  is set to 50 samples per peak to ensure that the grid sufficiently samples each peak (VanderPlas, 2018, Section 7.1). In the resulting PSD, the frequency with the highest peak is isolated, which corresponds to the frequency where the tidal signal (e.g., the spring-neap tidal cycle) is strongest in the sub-sampled time-series and is referred to as the 'peak tidal frequency'. Note that the spring-neap cycle has a period of 14.8 days but is subject to aliasing when sampled at an 8-day interval resulting in a peak at 17.5 days (refer Supporting Information S3 in Vos et al., 2020).

**Response to c):** the 0-days interval are present in areas of *path overlap* (overlap between images along the same path), while the 7-days interval are areas of *row overlap* (overlap between two adjacent rows).

**Response to d):** the outlier removal step is important as outliers can introduce errors in the computation of the spectra. Note that the `SDS_slope.reject_outliers()` function that is commented in the Jupyter notebook is setup for Narrabeen-Collaroy (a microtidal environment) and is not valid for Cable Beach (macrotidal). We created an *ad hoc* despiking algorithm which looks to remove points in the shoreline time-series that are physically impossible. For example, a sandy beach can be expected to erode of tens or even hundreds of metres in one timestep as a result of storm erosion (or accrete as a result of a nourishment or sand deposition), however it will take time to

recover that beach width, so if we have a spike in the time-series where the shoreline eroded X metres and accreted X metres in the next timestep, this has to be a false detection. The parameter regulating this distance X is the ``max_cross_change`` despiking parameter and is adjusted as a function of tidal range to allow for the tidal excursion for consecutive images acquired at different tidal stages. Hence the parameter is set to 40 m for beaches with a spring tidal range below 3 m and then follows a linear relationship as shown in Figure 3 (this relationship assumes tidal excursion with a slope of 0.02 to be conservative). According to this relationship ``max_cross_change`` should be 300 m for Cable Beach, which leads to 0 outliers being removed in the Jupyter notebook.

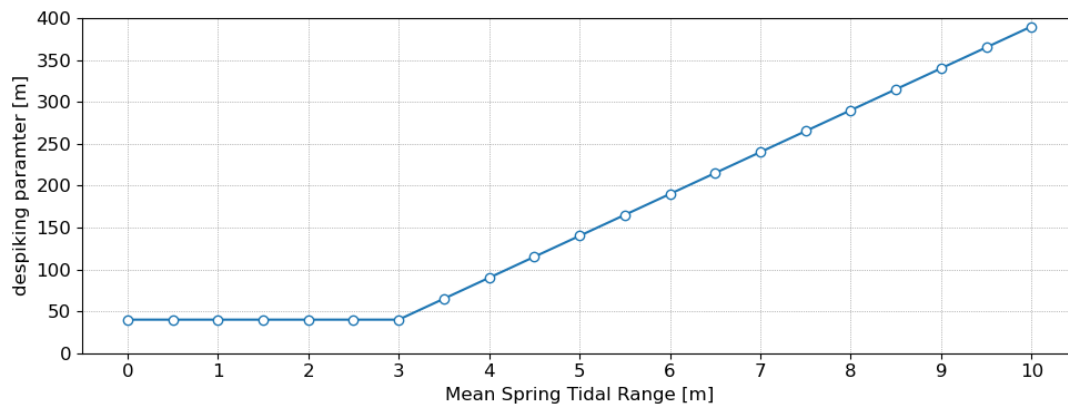


Figure 3. Relationship between the value of the despiking parameter and the Mean Spring Tidal Range.

We have added a short sentence to describe this step at **lines 94-95**:

Any outliers in the shoreline time-series (e.g., due to false detections) are also removed using a despiking algorithm.

And guided the readers to the Jupyter notebook examples for full details on the applied methodology, **lines 109-110**:

A full example of this procedure is presented for both a microtidal site (Narrabeen-Collaroy) and a macrotidal site (Cable Beach) in the form of Jupyter notebooks at <https://github.com/kvos/CoastSat.slope> (Vos, 2021b).

## 1.2. Limitations

**Response to a) and b):**

We thank the reviewer for this very good point, which we had not considered before. We agree with the referee that, based on the reasoning and references mentioned, Australia is a very favourable location for optical remote sensing with Landsat images.

We have added a paragraph in the discussion section following the referee's reasoning, stressing the limitations associated with applying this method in other geographical areas due to image availability in the Landsat archive and cloud frequency.

**Lines 257-262:**

While the focus of this dataset is on the Australian coastline, the generic nature of the method and global extent of Landsat imagery means that such a dataset could also be theoretically reproduced elsewhere. It is important to note however that the density of Landsat coverage is not consistent globally (Wulder et al., 2016) and that Australia (along with North America and Eastern China) has

some of the highest coverage in terms of image density. Additionally, the Australian continent is characterised by a relatively low mean cloud frequency (Wilson and Jetz, 2016), which means that a lower proportion of optical images are hindered by clouds. Other areas with a sparser Landsat coverage and/or higher cloud frequency, may not have the same temporal depth of shoreline observations, which could hinder the applicability of this method in some regions.

### 1.3. Data structure

**Response to a):** we have renamed all the fields using underscores and lower cases consistently.

**Response to b):** we have adjusted Tables 1 and 2 to match the identifiers in the dataset.

**Response to c):** it is a good suggestion to integrate the dataset into a database format. For the moment we think that a geospatial layer is suitable for the coastal sciences audience, which is more likely to import it into QGIS, but will consider the STAC framework for future developments.

## 2. Specific comments

- 2.1. The initial transect dataset was downloaded in 2018, and since it was quality-controlled and trimmed by manual digitalisation, we could not reproduce it automatically for the 2021 version of the OSM database.
- 2.2. This is a good question, while we are not experts in signal processing, our understanding is that a Discrete Fourier Transform (DFT) requires a convolution over different windows which will be distorted by the irregular sampling frequency. VanderPlas, (2018) discusses this issue in *Section 4. Nonuniform sampling*. While this issue can be mitigated by densely sampling the signal, albeit non-uniformly, this is not possible in our case as we must work with relatively large sampling intervals (days to weeks). The Lomb-Scargle transform is a least-squares spectral method that was specifically developed by astronomers to characterise periodicity in unevenly sampled time-series from optical sensors. It also has the advantage that we can define the frequency grid (limits and spacing), rather than it be dictated by the number of samples as in DFT/FFT. This is useful in our application as we can set a fine grid spacing around the frequencies of interest (i.e., fortnightly cycle) to fully capture those peaks and make sure they do not fall between grid points.

## 3. Technical corrections

### 3.1. Textual

We thank the referee for the suggestions, we have been incorporated them into the revised manuscript.

The last section of the manuscript (previously *Discussion and Outlook*) was split into a Discussion section (3 paragraphs) and a concise one-paragraph Conclusion.

**Discussion (lines 238-262):**

This new beach-face slope dataset provides full coverage of the Australian sandy coast, with beach-face slope estimates for 132,000 transects spaced every 100 m and extending along 13,200 km of coast. By focusing on the beach-face slope (defined between MSL to MHWS), it complements an existing dataset (Athanasidou et al., 2019) of nearshore slopes that are defined for the lower beach

profile (between MSL and the depth of closure). While the nearshore slopes can be used to transform offshore wave parameters to the nearshore (see Figure 1), the beach-face slope is necessary to predict the elevation of wave run-up and total swash excursion at the shoreline that is used in most standard wave runup formulations (e.g., Stockdon et al., 2006). Consequently, this beach-face slope dataset is an important step towards improving predictions of wave run-up and potential inundation hazards along the Australian coast (O’Grady et al., 2019). Additionally, coastal flood warning systems (e.g., Doran et al., 2015; Leaman et al., 2021; Stokes et al., 2019) often rely on a measure of the uncertainty associated with the input parameters to provide meaningful predictions with a margin of error. In that regard, the confidence bands associated with the beach-face slope estimates in this dataset can be used to propagate the uncertainty into the wave run-up equations and generate ensemble forecasts of total run-up elevation and swash excursion.

As identified in previous validation at 8 diverse sites (Vos et al., 2020), this dataset provides a good estimate of the ‘typical’ or long-term average beach-face slope obtained from 20 years of Landsat imagery. It is recognised however that the beach-face slope can vary quite substantially through time, particularly for microtidal intermediate beaches (such as those found in SE Australia) where the beach often rapidly transitions between morphodynamic beach states (Wright and Short, 1984). While estimating this temporal variability is challenging using the described method on the historic Landsat data (as undertaken here), new satellite remote sensing capabilities may make this a future possibility. For example, by combining satellite missions such as Landsat, Sentinel-2 (5-days revisit at the equator) and Planet’s CubeSat imagery (Kelly and Gontz, 2019), it might be possible to significantly increase the sampling frequency of shoreline observations. This higher-frequency data would enable a narrower time-window in which beach-face slopes are estimated to be used, potentially opening up the possibility to estimate temporal variability in beach-face slopes at different timescales (e.g., inter-annual and seasonal).

While the focus of this dataset is on the Australian coastline, the generic nature of the method and global extent of Landsat imagery means that such a dataset could also be theoretically reproduced elsewhere. It is important to note however that the density of Landsat coverage is not consistent globally (Wulder et al., 2016) and that Australia (along with North America and Eastern China) has some of the highest coverage in terms of image density. Additionally, the Australian continent is characterised by a relatively low mean cloud frequency (Wilson and Jetz, 2016), which means that a lower proportion of optical images are hindered by clouds. Other areas with a sparser Landsat coverage and/or higher cloud frequency, may not have the same temporal depth of shoreline observations, which could hinder the applicability of this method in some regions.

#### **Conclusion (lines 264-276):**

This study presents a new dataset of beach-face slopes for the Australian coastline derived from a newly available remote sensing technique. The dataset covers a total of 13,200 km of sandy coast and provides an estimate of the beach-face slope from Mean Sea Level (MSL) to Mean High Water Spring (MHWS) spaced every 100 m alongshore. Based on the width of the confidence bands around each slope estimate, it is found that 56% of the continental-scale dataset is classified as high confidence, while 23% have medium confidence and 21% have low confidence.

The dataset offers a unique view of large- to local-scale scale features in beach-face slope variability, providing data in regions with no in situ observational coverage. This new data availability opens up many interesting applications in coastal sciences and engineering, including:

- i) estimates (with confidence bands) of the beach-face slope parameter that is needed to predict wave run-up in coastal inundation forecasting systems (O'Grady et al., 2019);
- ii) enhanced understanding of large-scale geologic factors contributing to the distribution of beach-face slopes and sediment grain sizes (Bujan et al., 2019; Short, 2020);
- iii) informing coastal management and planning at the embayment scale;

The data is available in a simple format that can be readily imported into standard Geographical Information System software (e.g., QGIS, ArcGIS), or accessed programmatically, for use by coastal researchers and end-users.

## **ESSD-2021-388 – RC2 comment by Giovanni Scicchitano**

We would like to thank the referee for their positive comments and suggestion for improving the discussion/conclusion parts.

We have restructured the last section (Discussion and Outlook) and split it into a 3-paragraph Discussion and one-paragraph Conclusion.

Discussion (**lines 238-262**):

This new beach-face slope dataset provides full coverage of the Australian sandy coast, with beach-face slope estimates for 132,000 transects spaced every 100 m and extending along 13,200 km of coast. By focusing on the beach-face slope (defined between MSL to MHWS), it complements an existing dataset (Athanasίου et al., 2019) of nearshore slopes that are defined for the lower beach profile (between MSL and the depth of closure). While the nearshore slopes can be used to transform offshore wave parameters to the nearshore (see Figure 1), the beach-face slope is necessary to predict the elevation of wave run-up and total swash excursion at the shoreline that is used in most standard wave runup formulations (e.g., Stockdon et al., 2006). Consequently, this beach-face slope dataset is an important step towards improving predictions of wave run-up and potential inundation hazards along the Australian coast (O’Grady et al., 2019). Additionally, coastal flood warning systems (e.g., Doran et al., 2015; Leaman et al., 2021; Stokes et al., 2019) often rely on a measure of the uncertainty associated with the input parameters to provide meaningful predictions with a margin of error. In that regard, the confidence bands associated with the beach-face slope estimates in this dataset can be used to propagate the uncertainty into the wave run-up equations and generate ensemble forecasts of total run-up elevation and swash excursion.

As identified in previous validation at 8 diverse sites (Vos et al., 2020), this dataset provides a good estimate of the ‘typical’ or long-term average beach-face slope obtained from 20 years of Landsat imagery. It is recognised however that the beach-face slope can vary quite substantially through time, particularly for microtidal intermediate beaches (such as those found in SE Australia) where the beach often rapidly transitions between morphodynamic beach states (Wright and Short, 1984). While estimating this temporal variability is challenging using the described method on the historic Landsat data (as undertaken here), new satellite remote sensing capabilities may make this a future possibility. For example, by combining satellite missions such as Landsat, Sentinel-2 (5-days revisit at the equator) and Planet’s CubeSat imagery (Kelly and Gontz, 2019), it might be possible to significantly increase the sampling frequency of shoreline observations. This higher-frequency data would enable a narrower time-window in which beach-face slopes are estimated to be used, potentially opening up the possibility to estimate temporal variability in beach-face slopes at different timescales (e.g., inter-annual and seasonal).

While the focus of this dataset is on the Australian coastline, the generic nature of the method and global extent of Landsat imagery means that such a dataset could also be theoretically reproduced elsewhere. It is important to note however that the density of Landsat coverage is not consistent globally (Wulder et al., 2016) and that Australia (along with North America and Eastern China) has some of the highest coverage in terms of image density. Additionally, the Australian continent is characterised by a relatively low mean cloud frequency (Wilson and Jetz, 2016), which means that a lower proportion of optical images are hindered by clouds. Other areas with a sparser Landsat coverage and/or higher cloud frequency, may not have the same temporal depth of shoreline observations, which could hinder the applicability of this method in some regions.

Conclusion (**lines 264-276**):

This study presents a new dataset of beach-face slopes for the Australian coastline derived from a newly available remote sensing technique. The dataset covers a total of 13,200 km of sandy coast and provides an estimate of the beach-face slope from Mean Sea Level (MSL) to Mean High Water Spring (MHWS) spaced every 100 m alongshore. Based on the width of the confidence bands around each slope estimate, it is found that 56% of the continental-scale dataset is classified as high confidence, while 23% have medium confidence and 21% have low confidence.

The dataset offers a unique view of large- to local-scale scale features in beach-face slope variability, providing data in regions with no in situ observational coverage. This new data availability opens up many interesting applications in coastal sciences and engineering, including:

- i) estimates (with confidence bands) of the beach-face slope parameter that is needed to predict wave run-up in coastal inundation forecasting systems (O'Grady et al., 2019);
- ii) enhanced understanding of large-scale geologic factors contributing to the distribution of beach-face slopes and sediment grain sizes (Bujan et al., 2019; Short, 2020);
- iii) informing coastal management and planning at the embayment scale;

The data is available in a simple format that can be readily imported into standard Geographical Information System software (e.g., QGIS, ArcGIS), or accessed programmatically, for use by coastal researchers and end-users.

## ESSD-2021-388 – CC1 comment by Robbi Bishop-Taylor

We would like to thank Dr. Bishop-Taylor for the careful and thorough reading of this manuscript and for the thoughtful comments and constructive suggestions.

We did indeed followed the concept of tidal aliasing by sun-synchronous sensors that was introduced in the previous work by Bishop-Taylor et al. (2019) and were happy to find very similar patterns (with as low as 70% of tidal coverage, equivalent to the 30% bias reported in their analysis).

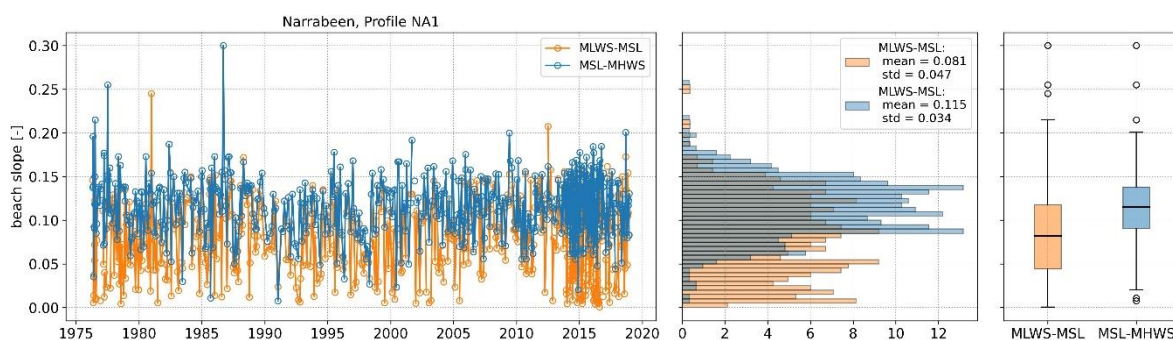
It is a very good suggestion to complement the % *MSTR observed* with the actual range of tidal elevations that are covered by the Landsat imagery. We have included this as additional metadata in the dataset (*min\_tide\_obs* and *max\_tide\_obs*) and agree that this will provide useful information to end-users.

There a several reasons why we believe that the beach-face slope estimated with our method is a proxy for the slope from MSL to MHWS, rather than from MLWS to MHWS, we have provided our arguments below and have clarified it in the manuscript to the benefit of the readers.

Initially, when we performed the validation against *in situ* surveys (across 8 sites with long-term survey data), we found that the slope estimates obtained with our algorithm matched best with the MSL to MHWS slope, while they tended to overestimate the MLWS to MHWS. While this observation is only data-driven, there is a physical rationale to support it.

Firstly, the beach-face is usually not linear (as assumed in our method) but rather concave and therefore can be described by two slopes, a steeper upper beach-face slope (MSL to MHWS) and a flatter lower beach-face slope (MLWS to MSL). The upper part tends to be more stable over time, while the lower beach-face slope is very dynamic as surfzone bars detach and attach to the shoreline, making it suddenly steeper or flatter (Wright and Short, 1984). For example, a transition from an intermediate state (e.g., transverse bar and rip) to a low tide terrace will drastically change the lower beach-face slope, but only affect the upper beach-face slope to a lesser extent.

To illustrate this point, the figure below shows the measured 40-year time-series for the lower (MLWS-MSL) and upper (MSL-MHWS) beach-face slopes at Narrabeen-Collaroy (Profile 1). You can see how the MLWS-MSL slope (orange) is flatter and more noisy (i.e., wider distribution) than the MSL-MHWS slope.



Therefore, we believe that this may explain why the resulting long-term slope estimate from our algorithm matches better with the beach-face slope (MSL to MHWS) which is more stable over time and a better representation of the 'typical' beach-face slope for that site. Unfortunately, the resolution of the publicly available images is not fine enough to estimate both the upper and lower beach-face slope at our study sites, but this could become possible with higher resolution commercial sensors

(Planet Labs, Maxar etc). We believe that using MSL-MHWS as proxy for the beach-face slope is somewhat analogous to using the MHWS-contour to monitor shoreline changes instead of the MSL-contour which is more noisy (Castelle et al., 2014; Splinter et al., 2014).

A second point to consider, is that the algorithm uses astronomical tides to calculate the water levels at which the Landsat images were acquired. However, the instantaneous water levels are also affected by wave setup (along wave-dominated beaches) and/or wind setup (along tide-dominated beaches), which tend to add a positive bias to the astronomical predictions. While presently these effects cannot be incorporated at the continental-scale due to the lack of nearshore hydrodynamic data, they may also contribute to the fact that our slope estimates match better with the upper beach-face slope rather than the entire intertidal zone. A positive vertical bias is also used to adjust the CoastSnap-derived shorelines (Harley et al., 2019) and Argus-derived shorelines (Harley et al., 2011).

**Lines 115-119:**

The satellite-derived beach-face slope estimates were found to match best with the slope between MSL to MHWS ( $R^2 = 0.93$ , bias = 0.0), while they tended to overestimate the full intertidal (MLWS to MHWS) slope. This can be explained by the fact that the upper intertidal slope (MSL to MHWS) is generally more stable over time, while the lower intertidal slope (MLWS to MSL) is more variable as intertidal bars attach/detach to the shoreline (Wright and Short, 1984). Wave runup and setup effects that are not included in the global tide model also tend to skew the shoreline detection towards the upper part of the intertidal profile (e.g., Harley et al., 2019).

We also thank Dr. Bishop-Taylor for the technical corrections, we have documented the missing fields and reprojected the geospatial layers to WGS84 as suggested.

## References

- Bishop-Taylor, R., Sagar, S., Lymburner, L. and Beaman, R. J.: Between the tides: Modelling the elevation of Australia's exposed intertidal zone at continental scale, *Estuar. Coast. Shelf Sci.*, 223(October 2018), 115–128, doi:10.1016/j.ecss.2019.03.006, 2019.
- Castelle, B., Marieu, V., Bujan, S., Ferreira, S., Parisot, J., Capo, S., Sénéchal, N. and Chouzenoux, T.: Equilibrium shoreline modelling of a high-energy meso-macrotidal, *Mar. Geol.*, 347, 85–94, doi:10.1016/j.margeo.2013.11.003, 2014.
- Department of the Interior U.S. Geological Survey: Landsat 8 Data Users Handbook, Nasa, 8(June), 97 [online] Available from: <https://landsat.usgs.gov/documents/Landsat8DataUsersHandbook.pdf> (Accessed 10 January 2022), 2016.
- Harley, M. D., Turner, I. L., Short, A. D. and Ranasinghe, R.: Assessment and integration of conventional, RTK-GPS and image-derived beach survey methods for daily to decadal coastal monitoring, *Coast. Eng.*, 58(2), 194–205, doi:10.1016/j.coastaleng.2010.09.006, 2011.
- Harley, M. D., Kinsela, M., Garcia, E. S. and Vos, K.: Shoreline change mapping using crowd-sourced smartphone images, *Coast. Eng.*, 150, 175–189, doi:<https://doi.org/10.1016/j.coastaleng.2019.04.003>, 2019.
- Splinter, K. D., Turner, I. L., Davidson, M. A., Barnard, P., Castelle, B. and Oltman-Shay, J.: A generalized equilibrium model for predicting daily to inter-annual shoreline response A generalized equilibrium model for predicting daily to inter-annual shoreline response, *J. Geophys. Res. Earth Surf.*, 119, 1936–1958, doi:10.1002/2014JF003106, 2014.
- USGS: Landsat Collection 1 Level 1 Product Definition. [online] Available from: [https://landsat.usgs.gov/sites/default/files/documents/LSDS-1656\\_Landsat\\_Level-1\\_Product\\_Collection\\_Definition.pdf](https://landsat.usgs.gov/sites/default/files/documents/LSDS-1656_Landsat_Level-1_Product_Collection_Definition.pdf), 2017.
- VanderPlas, J. T.: Understanding the Lomb–Scargle Periodogram, *Astrophys. J. Suppl. Ser.*, 236(1), 16, doi:10.3847/1538-4365/aab766, 2018.
- Vos, K., Harley, M. D., Splinter, K. D., Walker, A. and Turner, I. L.: Beach Slopes From Satellite-Derived Shorelines, *Geophys. Res. Lett.*, 47(14), doi:10.1029/2020GL088365, 2020.
- Wright, L. D. and Short, A. D.: Morphodynamic variability of surf zones and beaches: A synthesis, *Mar. Geol.*, 56(1–4), 93–118, doi:10.1016/0025-3227(84)90008-2, 1984.
- Wulder, M. A., White, J. C., Loveland, T. R., Woodcock, C. E., Belward, A. S., Cohen, W. B., Fosnight, E. A., Shaw, J., Masek, J. G. and Roy, D. P.: The global Landsat archive: Status, consolidation, and direction, *Remote Sens. Environ.*, 185, 271–283, doi:10.1016/J.RSE.2015.11.032, 2016.